Computer Simulation of Convective and Diffusive Transport of Controlled-Release Drugs in the Vitreous Humor

Matthew S. Stay,[1] Jing Xu,[2] Theodore W. Randolph,[2] and Victor H. Barocas[1,3]

Received September 16, 2002; accepted September 23, 2002

Purpose. Biodistribution of drugs in the eye is central to the efficacy of pharmaceutical ocular therapies. Of particular interest to us is the effect of intravitreal transport on distribution of controlled-released drugs within the vitreous.

Methods. A computer model was developed to describe the three-dimensional convective-diffusive transport of drug released from an intravitreal controlled release source. Unlike previous studies, this work includes flow of aqueous from the anterior to the posterior of the vitreous. The release profile was based on *in vitro* release of gentamicin from poly(L-lactic acid) microspheres into vitreous.

Results. For small drugs, convection plays a small role, but for large (slower diffusing) drugs, convection becomes more important. For the cases studied, the predicted ratio of drug reaching the retina to drug cleared by the aqueous humor was 2.4 for a small molecule but 13 for a large molecule. Transport in neonatal mouse eye, in contrast, was dominated by diffusion, and the ratio decreased to 0.39.

Conclusions. The interaction among convection, diffusion, and geometry causes significant differences in biodistribution between large and small molecules or across species. These differences should be considered in the design of delivery strategies or animal studies.

KEY WORDS: ocular drug delivery; biodistribution; sustained release.

INTRODUCTION

The vitreous humor (or simply "vitreous") is the clear, avascular, gelatinous body that fills the large space bounded by the lens, ciliary body, aqueous humor, and retina in the eye. The vitreous is highly hydrated, containing about 98% water. The primary structural components, type II collagen and hyaluronic acid, occupy less than 1% of the total volume, but they form a physically-crosslinked network that provides mechanical integrity to the vitreous (1).

A number of diseases affecting the vitreous and retina, including proliferative vitreoretinopathy and endophthalmitis, are currently treated by drugs (2). The blood-vitreous barrier, however, allows only a small amount of drug to penetrate from the blood into the vitreous humor (3), making systemic treatment difficult. Ocular drugs are usually delivered topically as aqueous eye drop solution or by direct intravitreal injection. These delivery methods are inherently pulsed, with a short initial period of overdosing followed by a long period of underdosing (4). Repeated administrations are needed to maintain effective drug levels, resulting in an increased incidence of complication (5) and higher risk of poor patient compliance. Controlled release of a therapeutic agent from a biodegradable polymeric system presents an alternative to traditional treatment strategies that can overcome some of the problems associated with pulsed delivery. It has been shown experimentally that controlled-release systems are more effective, require less frequent administration, and reduce the pulsed release effects (6).

Many drugs have a narrow concentration window of effectiveness and may be toxic at higher concentration (7), so the ability to predict local drug concentrations is necessary for proper loading of the delivery system. Furthermore, since small-animal models are often used in drug delivery studies, one should understand how eye size affects biodistribution of controlled-release drugs.

In light of the importance of intravitreal drug distribution, several previous investigators have developed models of transport in the vitreous, as summarized in Table I. All existing models assumed that the vitreous was stagnant. Our model relaxes this assumption and accounts for steady permeation of water through the vitreous humor. In addition, the new model allows for prediction of the biodistribution of drugs released from injectable biodegradable polymer microspheres (8). Permeation of water, although slow, is expected to affect significantly biodistribution of drugs, especially for high molecular weight (low diffusivity) molecules such as therapeutic antibodies.

Model Development

Both diffusive and convective mass transport within the vitreous were modeled, as described by the standard convection-diffusion-generation equation:

$$\frac{\partial c}{\partial t} + v \cdot \nabla c - D\nabla^2 c - q = 0 \tag{1}$$

where c is the concentration of drug, D is the (constant) diffusion coefficient, v is the velocity of the solvent (water), and q is the release rate as a function of position and time. Although the vitreous is compressible, we assume that no significant compression occurs under normal conditions, so the incompressible porous medium (Darcy flow) equations apply:

$$v = -\frac{K}{\mu}\nabla P \qquad \nabla \cdot v = 0 \Rightarrow \nabla^2 P = 0 \tag{2}$$

where K is the permeability of the vitreous humor, μ is the viscosity of the permeating aqueous humor, and P is the pressure.

We have developed technology for efficiently encapsulating hydrophilic drugs into microparticles of the hydrophobic polymer poly(L-lactic acid) (8) and have tested these microparticulate drug delivery systems in animal models as possible formulations for the treatment or prophylaxis of osteomyelitis (9–11). In the current application, microparticulate controlled release systems may provide significant advantages for intravitreal delivery of drugs, including the ability to

[1] Graduate Program in Scientific Computation, University of Minnesota, Minneapolis, Minnesota 55455.

[2] Department of Chemical Engineering, University of Colorado, Boulder, Colorado 80309-0424.

[3] To whom correspondence should be addressed. (e-mail: baroc001@umn.edu)

0724-8741/03/0100-0096/0 © 2003 Plenum Publishing Corporation

Table I. Models of Intravitreal Mass Transport

Geometry	Drug source	Other features	Source
Sphere	Injection (center)	Analytical solution	(15)
Spherical Shells	Continuous (exterior)	Used to fit experimental blood-vitreous permeation data	(28,29)
Modified Cylinder	Injection (center)	Included metabolism of injected drug	(14)
Anatomical (Rabbit or Human)	Injection (various locations)	Included elimination via aqueous humor	(16,30)
Anatomical (Mouse or Human)	Sustained release, point source	Includes active transport terms, convective terms	Current work

administer the dose through very fine needles and provide sustained drug release.

Since we are interested primarily in controlled release from very small (1 μm) spheres (8), we have modeled the source term q in Eq. (1) as a localized source. Previously, we studied release of gentamicin into cadaveric bovine vitreous and observed square-root-of-time kinetics with negligible initial burst for the release of the first 80% of the total loading (12). Similar square-root-of-time release was also observed in a number of other *in vitro* experiments (8,9). Thus, for the purposes of this computational study, we introduced a drug release term of the following form:

$$q = \frac{M_0\, k}{\sqrt{t}} \varphi\,(x,y,z) \tag{3}$$

where k is a rate constant for the release, M_0 is the total loading of drug in the particle, and φ is a function that is zero over most of the domain but rises sharply in the release volume (for convenience, one of the finite element basis functions was used, giving a release volume approximately 500 μm across in the human and 40 μm across in the mouse). The release function φ is normalized so that its volume integral is unity. The form of Eq. (3) gives a cumulative release profile of

$$Q = 2\, M_0\, k \sqrt{t} \tag{4}$$

We limited the analysis to 80% release. We further assumed, based on our *in vitro* experiments that the particles do not migrate significantly within the vitreous (12). The square-root-of-time form of the release profile that we have chosen is intended to be generally representative of diffusive release of drugs from spherical particles (9). It should be noted, however, that if the release profile were limited by external mass transfer (e.g., a drug only sparingly soluble in the vitreous), this form might over-predict drug release at early times.

Model Parameters

Our work with acid orange 8 (M_W = 364.4, D = 3.4 × 10^{-6} cm^2/s), and published studies of dexamethasone sodium m-sulfabenzoate ($M_W \approx 600$, D = 5.1 × 10^{-6} cm^2/s), and fluorescein (M_W = 332.3, D = 4.8-6.0 × 10^{-6} cm^2/s), suggest that the diffusion coefficient for 300-600 Da molecules is 60–75% of the value in water (13–15). For this work, we considered two possible diffusion coefficients, 5 × 10^{-6} cm^2/s (small molecule) and 1 × 10^{-7} cm^2/s (large molecule, e.g., an antibody). The hydraulic conductivity, defined as the permeability through the vitreous humor divided by the viscosity of the permeating liquid, is needed to describe the convective transport. We used a hydraulic conductivity of 8.4 × 10^{-7} $cm^2/(Pa{\cdot}s)$ based on our previous experiments on bovine vitreous (13). Analysis of previous results (12) for release of gentamicin from poly-(L-lactic acid) microspheres in cadaveric bovine vitreous gave a k value of 0.057 $day^{-1/2}$ and a release period of 50 days (80% release). We assumed an initial loading M_0 of 500 μg.

Boundary Conditions

The most challenging aspect of the model was the identification of the appropriate boundary conditions (BCs). Since we have second-order equations in concentration and pressure [Eqs. (1) and (2)], we require one concentration/flux condition and one pressure/permeation condition along each boundary. The model domain, which is identical to that previously used by Friedrich *et al.* (16) is shown in Fig. 1. The domain is bounded by the lens (L), the hyaloid membrane and the aqueous humor (H), and the retina and sclera (R). Since we consider cases in which the drug source was not along the axis of symmetry, the model was solved in its fully three-dimensional form. Figure 1 also shows the location of the source in the human and neonatal mouse cases.

The lens is avascular and highly compacted, making it essentially impermeable to water and to many drugs. The corresponding boundary conditions are

$$n \cdot \nabla P = 0 \quad \text{(no aqueous permeation into the lens)} \tag{5}$$

$$n \cdot \nabla c = 0 \quad \text{(no drug permeation into the lens)} \tag{6}$$

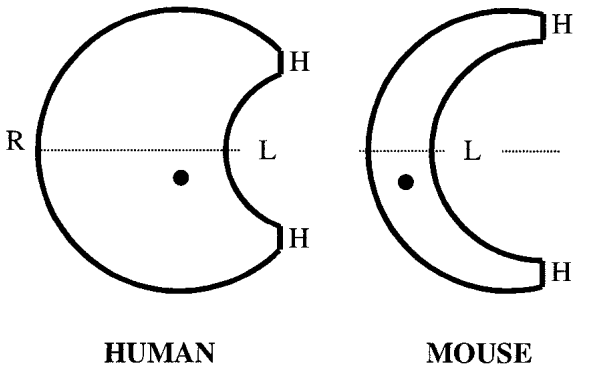

Fig. 1. Domain of vitreous transport model. The domain for the human eye, which is identical to that used in (16), represents the entire vitreous gel. It is bounded by the lens (L), the hyaloid membrane and beyond it the aqueous humor (H), and the retina and sclera (R). Location of the release source and the domain of the simulated mouse eye are shown. The radii of curvature of the retina and lens in the human eye are taken to be 0.85 cm and 0.55 cm, respectively. The center of curvature of the retina is 0.61 cm posterior to the hyaloid membrane boundary, and the center of curvature of the lens is 0.24 cm anterior to the hyaloid membrane. For the neonatal mouse, the radii of curvature of retina and lens are 0.054 and 0.042 cm, respectively, the center of curvature of the lens is coplanar with the hyaloid membrane, and the center of curvature of the vitreous is 0.012 cm posterior to the hyaloid membrane.

where n is the outward-pointing normal at the retinal surface, and Eq. (6) makes use of the fact that the normal velocity of the aqueous must be zero by Eq. (5).

The hyaloid membrane separates the vitreous humor from the aqueous humor and the anterior segment of the eye. Because the hyaloid membrane is relatively thin and highly porous, we assumed no resistance to flow across it, implying that the pressure at the posterior hyaloid surface is equal to the pressure in the aqueous humor, which is equivalent to the routinely-measured intraocular pressure (IOP). For a healthy patient, IOP is generally between 15 and 20 mmHg (2000–2600 Pa), whereas for a glaucoma patient it can be twice that. We chose 2000 Pa as the IOP and thus set $P = 2000$ Pa at the hyaloid. We further assumed that the hyaloid exerts no significant resistance to passive transport of drug from the vitreous humor to the aqueous humor. The aqueous humor has a residence time in the eye of about 2.5 hr (1). Since we are concerned with drug release taking place over weeks, we assumed that the aqueous turnover was fast enough to remove all drug as it arrives, and we set $c = 0$ at the hyaloid.

The retina and sclera present some difficulty in the formulation of correct boundary conditions. In light of the wide range of experimental results, we included passive transport terms in both the pressure and the species balance equations and active species transport:

$$n \cdot v = n \cdot \left(-\frac{K}{\mu} \nabla P \right) = K_P (P - P_V) \tag{7}$$

$$n \cdot (-D\nabla c + vc) = (R_{act} + K_C)c \tag{8}$$

where K_P [$= 5 \times 10^{-10}$ cm/(Pa·s)] is the hydraulic conductivity of the retina and sclera, and P_V ($= 1200$ Pa) is the pressure of the vein downstream of the flow. For the concentration boundary condition, we combined the passive (K_C) and active (R_{act}) transport terms to yield $(R_{act} + K_C) = 10^{-5}$ cm/s. A discussion of the existing data on transport out of the vitreous, including the rationale for Eqs. (7) and (8) and the values of the parameters, is included in the Appendix.

Solution Method

Equations (1) and (2) were solved in series using the standard Galerkin finite element method (FEM) with piecewise triquadratic basis functions for the pressure and concentration. FEM works well for elliptic problems on oddly-shaped domains, and it accommodates flux boundary conditions in a natural way. An *ad hoc* finite element code was developed and run on an 800-MHz Pentium III microcomputer running Linux.

The first stage of the solution process was the solution of the steady-state Darcy Eq. (2). This solution was assumed to be time-independent and to be unaffected by the action of the diffusing drug. Since Eq. (2) is quasi-steady, the assumption of constant pressure/velocity profile could be relaxed by simply recalculating the profile at each time step. For the current analysis, however, the constant profile assumption was used, so the pressure profile was calculated once *a priori* and used in the solution of the transient delivery problem.

The conservation of drug Eq. (1) was subsequently solved by the method of lines. The spatial derivatives were discretized by FEM, and the resulting ordinary differential equation was solved by implicit Euler integration.

RESULTS

Intraocular Pressure and Velocity Profiles

As noted above, the first step in the simulation process was the determination of the pressure and velocity profiles within the vitreous at steady state. Figure 2 shows the FEM solution of Eq. (2). The pressure is, as specified, highest at the aqueous border, and it decreases monotonically through the vitreous. The model predicts a steady permeating flow down the pressure gradient from the anterior to the posterior vitreous. The average velocity at the retinal surface is 4.0×10^{-7} cm/s, and the total volumetric flow rate through the vitreous is 0.14 μL/min. The pressure drop across the vitreous is less than 1 Pa, indicating that almost all of the pressure drop between the aqueous humor (2000 Pa) and the eventual drainage into a vein (1200 Pa) occurs across the sclera, consistent with earlier analysis (17).

Intraocular Drug Release and Biodistribution

Figure 3 shows the concentration of drug at the vitreous-retina surface (as viewed from behind the retina) at 1, 5, 10, and 20 days after release. As expected, there is an early lag as the drug requires finite time to be transported to the retinal surface. At long time, the square-root-of-time release profile dies out, and the concentration decays accordingly.

Our model also predicts the gross biodistribution of drug with time. Neglecting degradation and metabolism of drug within the vitreous, there are four possible drug locations:

1. Still in the microparticle
2. Released from the particle but still inside the vitreous
3. Cleared by the aqueous humor
4. Delivered to the retina (for the purpose of this study, any drug leaving the posterior vitreous was classified as delivered to the retina, regardless of its final destination)

The sum total of the mass of drug in each location must remain constant at the total loading. Figure 4 shows the cumulative distribution of a relatively small drug ($D = 5 \times 10^{-6}$ cm^2/s) over course of release. Since we have assumed square-root-of-time release kinetics and the various masses are plotted vs. the square root of time, the amount still in the particle decreases linearly on the graph. The drug mass in the vitreous increases early in the release but quickly decays as drug is absorbed by the retina or swept away by the aqueous. At the end of the 50-day simulated release period, there is relatively little drug still in the vitreous, and 70% of the released drug has reached the retina with 29% cleared by the aqueous.

Figure 5 shows two major effects as drug diffusivity decreases (i.e., for a larger drug). First, the amount of holdup in the vitreous is increased significantly because of the slower diffusion. Second, because of the increased significance of convection relative to diffusion, the distribution to the retina downstream of the convective flow is increased. Specifically, at the end of the release period, 83% of the drug has reached the retina and only 6% has been cleared by the aqueous, the remainder being still in the vitreous. Thus, the ratio of drug reaching the retina to drug reaching the aqueous increases from 2.4 to 13.

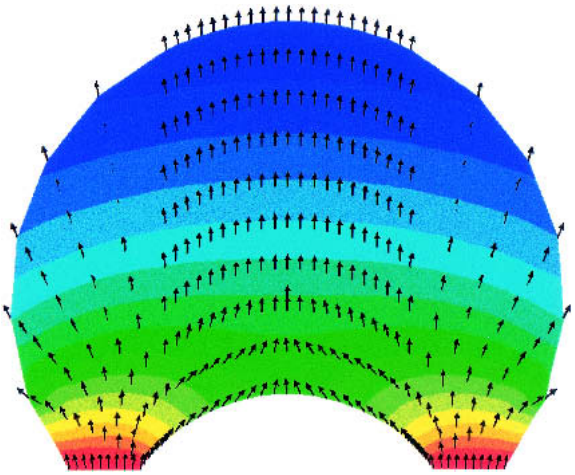

Fig. 2. Pressure and flow direction distribution in the vitreous. The pressure (indicated by color) drops less than 1 Pa between the hyaloid membrane and the anterior surface of the retina. As required by Eq. (2), the flow travels down the pressure gradient.

Because of the importance of the neonatal mouse model in the testing of pharmaceutical systems, we repeated the calculation of figure 4 for a mouse eye (geometry based on (18)) instead of a human eye. Figure 6 shows that there is essentially no hold-up in the vitreous because of its extremely small size. The limiting step in the delivery process is the release rate, and the amounts of delivery to the retina and loss to the aqueous are proportional to the amount released. Also of note is a significant reduction in convection away from the hyaloid toward the retina, with 71.7% of the released drug being lost and only 28.3% being delivered to the retina.

DISCUSSION

We have developed a model of controlled drug delivery to the vitreous humor. This model, unlike previous ones, accounts for transient release from a localized source, simulating microparticle delivery. The model also solves for the steady flow of aqueous humor permeating through the vitre-

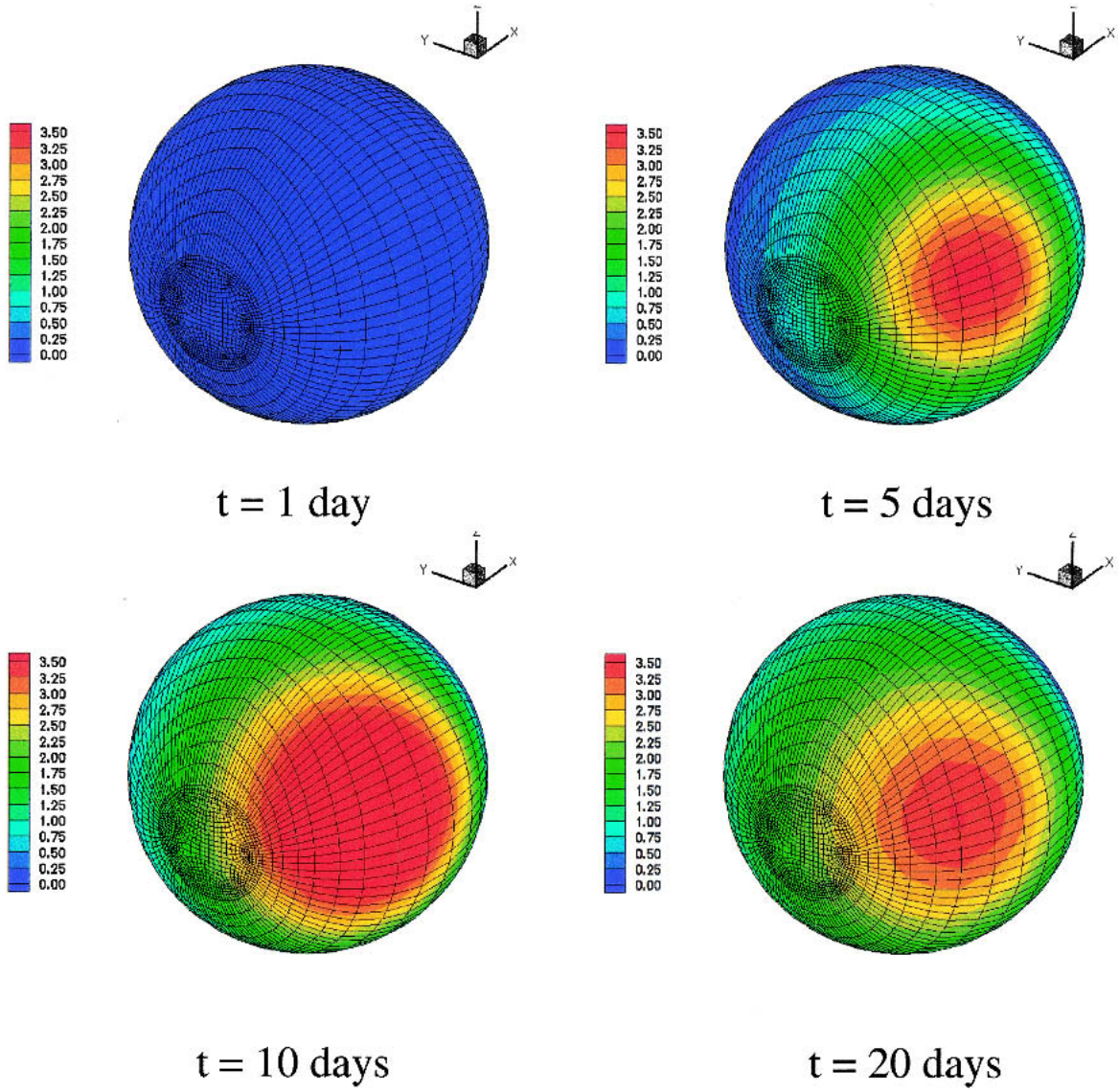

Fig. 3. Simulated release profile in the human eye. Posterior view of concentration distribution on the posterior vitreous surface at t = 1, 5, 10, and 20 days after implantation. Color bar shows concentration in $\mu g/cm^3$.

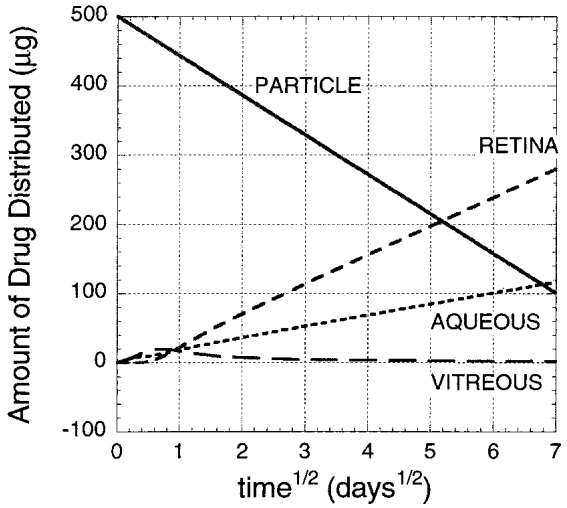

Fig. 4. Biodistribution of a small drug in the human eye. Drug has four possible locations: still in the particle, diffusing in the vitreous, lost across the hyaloid (and presumably cleared by the aqueous circulation), and delivered to the retina. The classification "delivered to the retina" includes all drug reaching the posterior vitreous surface, at which point drug may be metabolized by the retina, may pass through the retina and be cleared by the choroidal blood flow, or may diffuse across the sclera into the episcleral space. The plot shows how the four states are distributed over time for a relatively small drug ($D = 5 \times 10^{-6}$ cm^2/s). Note that the horizontal axis is square root of time.

ous from the aqueous humor to the retina. The model and its solution method are easily generalized, and the simulation could thus be used to study other drugs, reaction/metabolism of drug within the vitreous, disease states that affect ocular pressure or vitreous permeability, or multiple injection points, possibly with different loading or release rates. Also, because the velocity profile is calculated, one could modify the model to study feedback processes in which the drug affects aqueous humor flow in the vitreous, which in turn affects the distribution of drug. Although only one drug delivery location was considered in this study, the source point could be modified easily to accommodate other delivery locations.

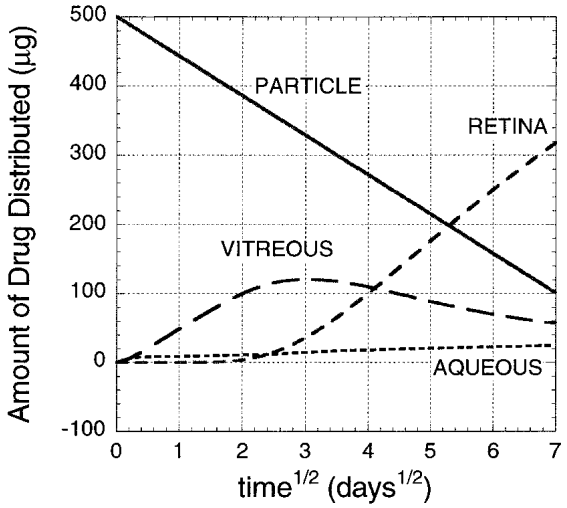

Fig. 5. Biodistribution of a large drug in the human eye. The biodistribution plot is for the same delivery location and rate as in Fig. 4, except that the diffusion coefficient has been reduced to 10^{-7} cm^2/s.

The model assumption that the lens is impermeable could be relaxed if one were interested in a drug capable of entering the lens (19). Because it is stagnant and cannot act as a "sink" in the way that the aqueous does, the lens would have to be included in the model by enlarging the domain rather than by a simple modification of the boundary conditions. Further, the model assumes that there is no net motion of the vitreous even though there is experimental evidence that the vitreous can move quite dramatically during eye motion, particularly the highly liquefied vitreous of the elderly (1). It may be more appropriate to consider a portion of the vitreous as intact, modeled as herein, and a portion as liquefied and well-mixed by ocular motion. The model also assumes an active drug transport term at the posterior vitreous surface based on fluorescein data (20,21); although the current model provides insight into large-drug vs. small-drug transport within the vitreous, care should be taken in generalizing the model results.

The most significant conclusion from the simulations was that the transport of drug within the human vitreous depends on both convection and diffusion, even for a small (MW = 364) and thus highly diffusive component like acid orange 8. Since intravitreal flow could depend significantly on intraocular (i.e., aqueous humor) pressure, which varies among individuals and is particularly high in glaucoma patients, one should be aware of intraocular pressure when developing an intravitreal delivery strategy. Our results are also consistent with Maurice's (22) observation that a needle hole in the sclera can affect transport between the aqueous and vitreous humors.

The behavior observed is readily analyzed by considering the Péclet number, which can be estimated for the three cases studied:

$$\text{Pé} = \frac{VL}{D} = \begin{cases} \dfrac{(3.8\times10^{-6}\ \text{cm/s})(1.43\ \text{cm})}{5\times10^{-6}\ \text{cm}^2/\text{s}} = 1.1 & \text{HUMAN, High D} \\ \dfrac{(3.8\times10^{-6}\ \text{cm/s})(1.43\ \text{cm})}{1\times10^{-7}\ \text{cm}^2/\text{s}} = 54.3 & \text{HUMAN, Low D} \\ \dfrac{(3.8\times10^{-6}\ \text{cm/s})(0.1\ \text{cm})}{5\times10^{-6}\ \text{cm}^2/\text{s}} = 0.076 & \text{MOUSE, High D} \end{cases} \tag{9}$$

The transport mechanism changes fundamentally between the human and neonatal mouse eyes. Transport is largely diffusive in the mouse, balanced between convection and diffusion for the small drug in the human, and largely convective for the large drug in the human. The practical significance of this difference lies in the relative partitioning of drug between its two possible destinations: the retina (the target) and the aqueous humor (leading to systemic elimination). This difference arises from the importance of intravitreal flow in the human eye, which convects drug toward the retina. The convection effect is exaggerated in the case of a relatively large (i.e., slowly-diffusing) drug.

In light of the contribution of convection to intravitreal transport in the human, the insignificance of convection in the neonatal mouse eye due to scaling should be considered in the design and analysis of animal model studies of ocular delivery. Since diffusion dominates in the small animal, the distribution of drug does not remain constant as animal size in-

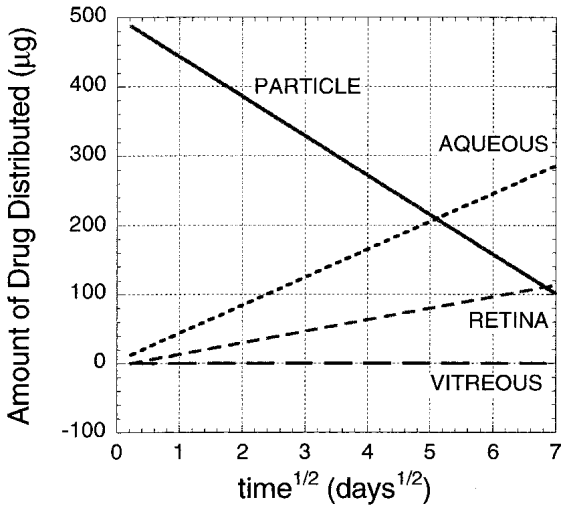

Fig. 6. Biodistribution in the mouse eye. The plot shows biodistribution data for release of a small drug into a neonatal mouse eye. The location of the release source is given in Fig. 1.

creases, but rather the large animals (e.g., humans) will have more efficient delivery to the retina and less peripheral distribution. Many drugs selected for controlled release are toxic at high dose, so awareness of the shift in transport mechanism between mouse and human is necessary.

ACKNOWLEDGMENTS

This work was supported by the Colorado RNA Center, the Colorado Institute for Research in Biotechnology, and by the Universities of Colorado and Minnesota. A supercomputing resources allocation grant from the University of Minnesota Supercomputing Institute for Digital Simulation and Advanced Computation is acknowledged.

APPENDIX

Boundary Conditions on the Retinal Surface

Appropriate boundary conditions on the retinal surface require that we specify how the fluxes of aqueous humor and of drug into the retinal surface depend on the local pressure and concentration. In the case of purely passive transport, a mixed linear boundary condition is sufficient to capture the relationships. In fact, the passive hydraulic conductivity of the sclera has been measured to be 5×10^{-10} cm/(Pa·s) (17). There is, however, considerable experimental evidence suggesting that active transport across the retinal pigment epithelium could be significant. Tsuboi and Pederson (23) showed that explanted retinal pigment epithelium can pump water from the vitreal to the scleral side *in vitro*. In light of the high flow resistance of the sclera, even a small active transport contribution could affect the flow field.

Since the fluid flow problem is assumed to be at steady state, conservation of mass requires that the total flow into the vitreous from the aqueous be equal to the total flow out of the vitreous across the retina. Posterior flow from aqueous to vitreous has been studied by various investigators, providing some insight into the appropriate retina/sclera boundary condition, although the nature of posterior flow and the possibly related uveoscleral outflow pathway remains cloudy (cf. (24)).

Maurice (22) concluded based on the ability of fluorescein to diffuse from the vitreous to the aqueous that any posterior flow must be very slow, much slower than the 0.5 mm/hr suggested earlier. Araie and co-workers subsequently found, however, that changes in intraocular pressure by artificially clogging the trabecular mesh (25) led to changes in transport across the aqueous-vitreous boundary, suggesting that there is a small but significant pressure-driven flow across the aqueous-vitreous boundary. Based on those results, we estimate that the posterior flow of aqueous into the vitreous is at most 10% of the total aqueous humor generated; in the human, this corresponds to a flow rate of approximately 0.25 μl/min, or a velocity of roughly 0.25 mm/hr, consistent with Maurice's conclusion. A short-time (40 min) study in rabbit (26) using radio-labeled water found no measurable flow of aqueous into the vitreous, but their resolution was only 0.5 mm, and a velocity of 0.25 mm/hr would be insufficient to produce a resolvable change within the 40-min experiment. A boundary condition with only passive terms,

$$n \cdot v = n \cdot \left(-\frac{K}{\mu} \nabla P \right) = K_P (P - P_V) \tag{7}$$

where the passive hydraulic conductivity K_P is set to 5×10^{-10} cm/(Pa·s) based on (17), produces an average aqueous humor velocity of 4.0×10^{-7} cm/s across the retina, which corresponds to a velocity of 3.8×10^{-6} cm/s (0.14 mm/hr) across the hyaloid. The volumetric flow rate is 0.17 μl/min, or 7% of the total aqueous humor production. We consider this a reasonable estimate of the aqueous flow rate through the vitreous based on existing experimental data, and we therefore neglected active water transport in this study.

Selecting the boundary condition for drug transport involves complications similar to those involved in selecting the flow boundary condition. There is a body of experimental evidence supporting the idea that there is active as well as passive transport of drugs out of the vitreous. Most compelling, the transport of fluorescein from the vitreous to the blood is as much as 100 times faster than the corresponding transport into the vitreous (20,21), a feature described generally as the blood-vitreous barrier (3). Since the unidirectionality is too great to be explained by the relatively small convective flow rates available, (20,21) conclude that there is active transport of fluorescein out of the vitreous, possibly by an anion pump. Those studies found no concentration dependence in the permeability, so we introduce a linear active transport term:

$$n \cdot (-D\nabla c + vc) = R_{act}\, c + K_C (c - c_V) \tag{A-1}$$

where R_{act} is the constant for active transport and K_C is the constant for passive transport. Since we only consider cases in which the downstream concentration $c_V = 0$, there is no practical distinction between K_C and R_{act}, and we write the final form of the concentration boundary condition:

$$n \cdot (-D\nabla c + vc) = (R_{act} + K_C)c \tag{8}$$

where the sum of the active and passive terms is equivalent to an effective permeability coefficient. Taking a sample-size-weighted average of the data summarized in Table II of (21), we estimate $K_C = 1.9 \times 10^{-7}$ cm/s and $R_{act} = 5.7 \times 10^{-6}$ cm/s;

a survey of other data on fluorescein transport into the retina (15,27–29) yields an estimate of the overall vitreous-retina permeability constant $K_C + R_{act} = 2 \times 10^{-5}$ cm/s, about a factor of three higher than the total based on (21). In light of the data, we set $K_C + R_{act} = 1 \times 10^{-5}$ cm/s for our simulations.

REFERENCES

1. W. M. Hart. *Adler's Physiology of the Eye*, Mosby-Year Book, Chicago, Illinois, 1992.
2. W. H. Stern, G. P. Lewis, P. A. Erickson, C. J. Guerin, D. H. Anderson, S. K. Fisher, and J. J. O'Donnell. Fluorouracil Therapy for Proliferative Vitreoretinopathy After Vitrectomy. *Am. J. Ophthalmol.* **96**:33–42 (1983).
3. G. M. Bleeker. N. J. V. Haeringen, E. R. Mass, and E. Glasius. Selective Properties of the Vitreous Barrier. *Exp. Eye Res.* **7**:37–46 (1968).
4. F. Q. Liang and R. S. Viola. M. d. Cerro, and V. Aquavella. Noncross-linked Collagen Discs and Cross-linked Collagen Shields in the Delivery of Gentamicin to Rabbits Eyes. *Invest. Ophthalmol. Vis. Sci.* **33**:2194–2198 (1992).
5. G. G. Giordano, M. F. Refojo, and M. H. Arroyo. Sustained Delivery of Retinoic Acid from Microspheres of Biodegradable Polymer in PVR. *Invest. Ophthalmol. Vis. Sci.* **34**:2743–2751 (1993).
6. H. Miyamoto, Y. Ogura, M. Hashizoe, N. Kunou, Y. Honda, and Y. Ikada. Biodegradable Scleral Implant for Intravitreal Controlled Release of Fluconazole. *Curr. Eye Res.* **16**:930–935 (1997).
7. S. C. Pflugfelder, E. Hernandez, and S. J. Fliesler. and J. Alvarez. Intravitreal Vancomycin. Retinal Toxicity, Clearance, and Interaction with Gentamicin. *Arch. Ophthalmol.* **105**:831–837 (1987).
8. R. T. Falk, T. W. Randolph, J. Meyer, R. Kelly, and M. Manning. Controlled Release of Ionic Compounds from Poly (L-lactide) Microspheres Produced by Precipitaion with a Compressed Antisolvent. *J. Control. Release* **44**:77–85 (1997).
9. J. D. Meyer, R. F. Falk, R. M. Kelley, J. E. Shively, S. J. Withrow, W. S. Dernell, D. J. Kroll, T. W. Randolph, and M. C. Manning. Preparation and In Vitro Characterization of Gentamicin-Impregnated Biodegradable Beads Suitable for Treatment of Osteomyelitis. *J. Pharm. Sci.* **87**:1149–1154 (1997).
10. W. Dernell, S. Withrow, M. Manning, C. Kuntz, R. Dewell, F. Garry, B. Powers, J. Shively, R. Falk, and T. Randolph. In Vivo Evaluation of Gentamicin-Impregnated Polylactic Acid Beads Implanted in Sheep. *J. Bioact. and Compat. Polym.* **16**:119–135 (2001).
11. W. Dernell, C. Gentry-Weeks, M. Manning, B. Powers, R. Park, M. Lafferty, C. Kuntz, J. Shively, R. Falk, J. Meyer, T. Randolph, and S. Withrow. In Vivo Evaluation of Anibiotic Impregnated beads in a Rat Osteomyelitis Model. *J. Bioact. Compat. Polym.* **16**:235–250 (2001).
12. J. Xu. Controlled release and the concentration distribution of the drug in the vitreous humor. M. S. Thesis in Chemical Engineering, University of Colorado, Boulder, Colorado, 1999.
13. J. Xu, J. J. Heys, T. W. Randolph, and V. H. Barocas. Permeability, and diffusion in the vitreous humor: Implications for controlled drug delivery. *Pharm. Res.* **17**:664–669 (2000).
14. A. Ohtori and K. J. Toko. In Vivo/In Vitro Correlation of Intravitreal Delivery of Drugs With the Help of Computer Simulation. *Biol. Pharm. Bull.* **17**:283–290 (1994).
15. M. Araie and D. Maurice. The Loss of Flourescein, Flourescein Glucuronide and Flourescein Isothiocyanate Dextran from the Vitreous by the Anterior and Retinal Pathways. *Exp. Eye Res.* **52**:27–39 (1991).
16. S. Friedrich, Y. Cheng, and B. Saville. Drug Distribution in the Vitreous Humor of the Human Eye: The Effect of Intravitreal Injection Position and Volume. *Curr. Eye Res.* **16**:663–669 (1997).
17. I. Fatt and B. Hedbys. Flow of water in the sclera. *Exp. Eye Res.* **10**:243–249 (1970).
18. W. G. Robison, T. Kuwabara, and J. Zwaan. Eye research. In H. L. Foster, J. D. Small, and J. G. Fox (eds.), *The Mouse in Biomedical Research. Volume IV. Experimental Biology and Oncology*, Academic Press, New York, 1982 pp. 69–89.
19. P. A. Pearson, G. J. Jaffe, D. F. Martin, G. J. Cordahi, H. Grossniklaus, E. T. Schmeisser, and P. Ashton. Evaluation of a delivery system providing long-term release of cyclosporine. *Arch. Ophthalmol.* **114**:311–317 (1996).
20. C. B. Engler, B. Sander, M. Larsen, P. Dalgaard, and H. Lund-Andersen. Fluorescein Transport Across the Human Blood Retina Barrier in the Direction Vitreous to Blood - Quantitative Assessment in- Vivo. *Acta Ophthalmol. (Copenh.)* **72**:655–662 (1994).
21. B. Moldow, B. Sander, M. Larsen, and H. Lund-Andersen. Effects of acetazolamide on passive and active transport of fluorescein across normal BRB. *Invest. Ophthalmol. Vis. Sci.* **40**:1771–1775 (1999).
22. D. Maurice. Flow of water between aqueous and vitreous compartments in the rabbit eye. *Am. J. Physiol.* **252**:F104–F108 (1987).
23. S. Tsuboi and J. E. Pederson. Effect of plasma osmolality and intraocular pressure on fluid movement across the blood-retinal barrier. *Invest. Ophthalmol. Vis. Sci.* **29**:1747–1749 (1988).
24. M. Johnson and K. Erickson. Mechanisms and routes of aqueous humor drainage. In D. M. Albert and F. A. Jakobiec (eds.), *Glaucoma*, W.B. Saunders: Philadelphia, Pennsylvania, 2000 pp. 2577–2594.
25. Y. Sugiura and M. Araie. Effects of intraocular pressure change on movement of FITC-dextran across vitreous-aqueous interface. *Jpn. J. Ophthalmol.* **33**:441–450 (1989).
26. H. M. Cheng, K. K. Kwong, J. Xiong, and B. T. Woods. Visualization of water movement in the living rabbit eye. *Graefes Arch. Clin. Exp. Ophthalmol.* **230**:62–65 (1992).
27. S. Koyano, M. Araie, and S. Eguchi. Movement of fluorescein and its glucuronide across retinal pigment epithelium-choroid. *Invest. Ophthalmol. Vis. Sci.* **34**:531–538 (1993).
28. A. Yoshida, M. Kojima, and S. Ishiko. Inward and outward permeability of the blood-retinal barrier. In J. Cunha-Vaz and E. Leite (eds.). *Ocular Fluorophotometry and the Future*, Kugler & Ghedini Publishers, Amsterdam, 1989, pp. 89–97.
29. A. Yoshida, S. Ishiko, and M. Kojima. Outward Permeability of Blood-Retinal Barrier. *Graefes Arch. Clin. Exp. Ophthalmol.* **230**:78–83 (1992).
30. S. Friedrich, B. Saville, and Y. Cheng. Finite Element Modeling of Drug Distribution in the Vitreous Humor of the Rabbit Eye. *Annals Biomed. Eng.* **25**:303–314 (1997).